Atomically bridged palladium between nickel species and carbon microfibers and the subsequent conversion into free-standing and electrocatalytically active multifunctional electrodes

Zahra Hagheh Kavousi,[a,b] Clémence Badie,[c] Vyshnav Kannampalli,[c] Massomeh Ghorbanloo,[b] Qing Wang,[c] Hazar Guesmi,[c] Lionel Santinacci,[d,e,*] Yaovi Holade,[a,e,f*] and Mikhael Bechelany[a,g*]

[a]Institut Européen des Membranes, IEM, UMR 5635, Univ Montpellier, ENSCM, CNRS, 34090 Montpellier, France

[b]Department of Chemistry, Faculty of Sciences, University of Zanjan, Zanjan, Iran

[c]Institut Charles Gerhardt Montpellier (ICGM) – UMR 5253, University of Montpellier, CNRS, 34090 Montpellier, France.

[d]Aix Marseille Univ, CNRS, CINaM, Marseille 13009, France

[e]French Research Network on Hydrogen (FRH2), Research Federation No. 2044 CNRS, BP 32229, 44322 Nantes Cedex 3, France, https://frh2.cnrs.fr/

[f]Institut Universitaire de France (IUF), 75005 Paris, France

[g]Functional Materials Group, Gulf University for Science and Technology (GUST), Mubarak Al-Abdullah 32093, Kuwait

Corresponding authors: lionel.santinacci@univ-amu.fr (L.S.), yaovi.holade@enscm.fr (Y.H.), and mikhael.bechelany@umontpellier.fr (M.B)

Table of Contents

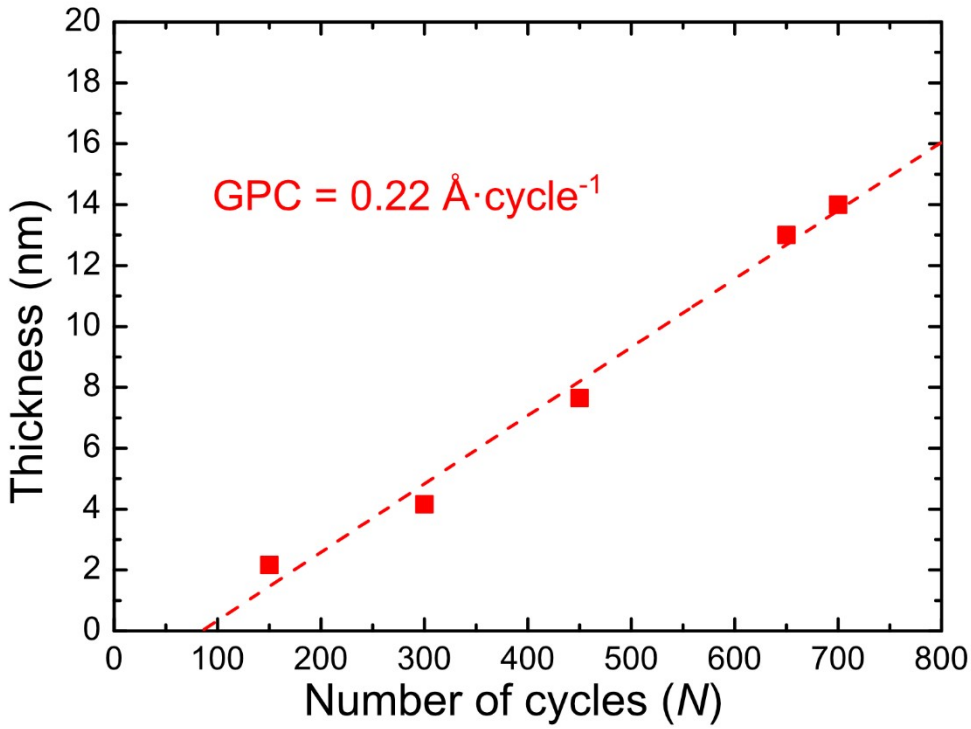

Figure S1. Dependencies of film thickness on number of ALD cycles for NiO_x films deposited on planar Si wafers.

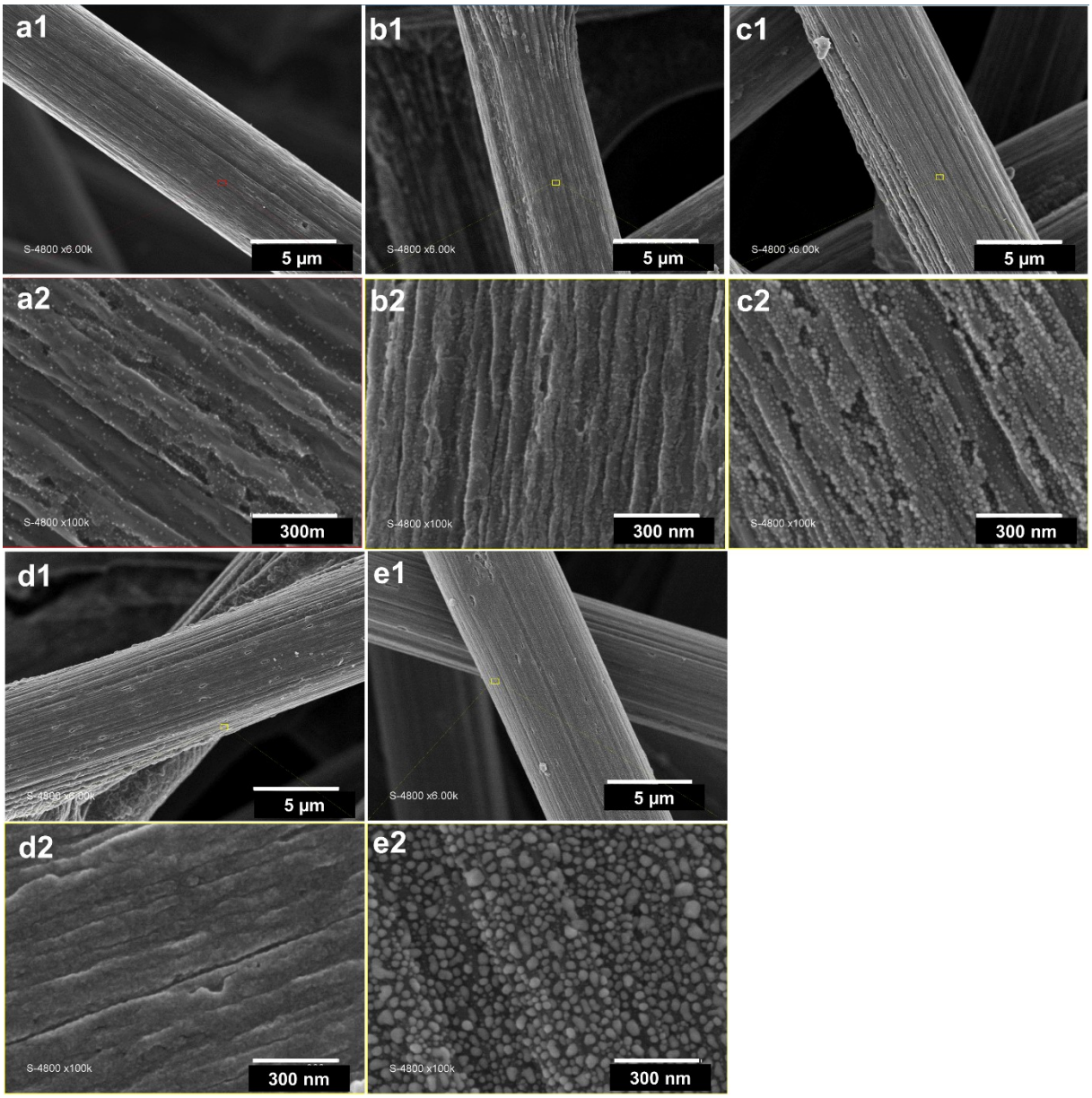

Figure S2. SEM images of a1-a2) GDE-Pd, b1-b2) GDE-Pd/NiO250, c1-c2) GDE-Pd/NiO250-TT, d1-d2) GDE-Pd/NiO1000 and e1-e2) GDE-Pd/NiO1000-TT.

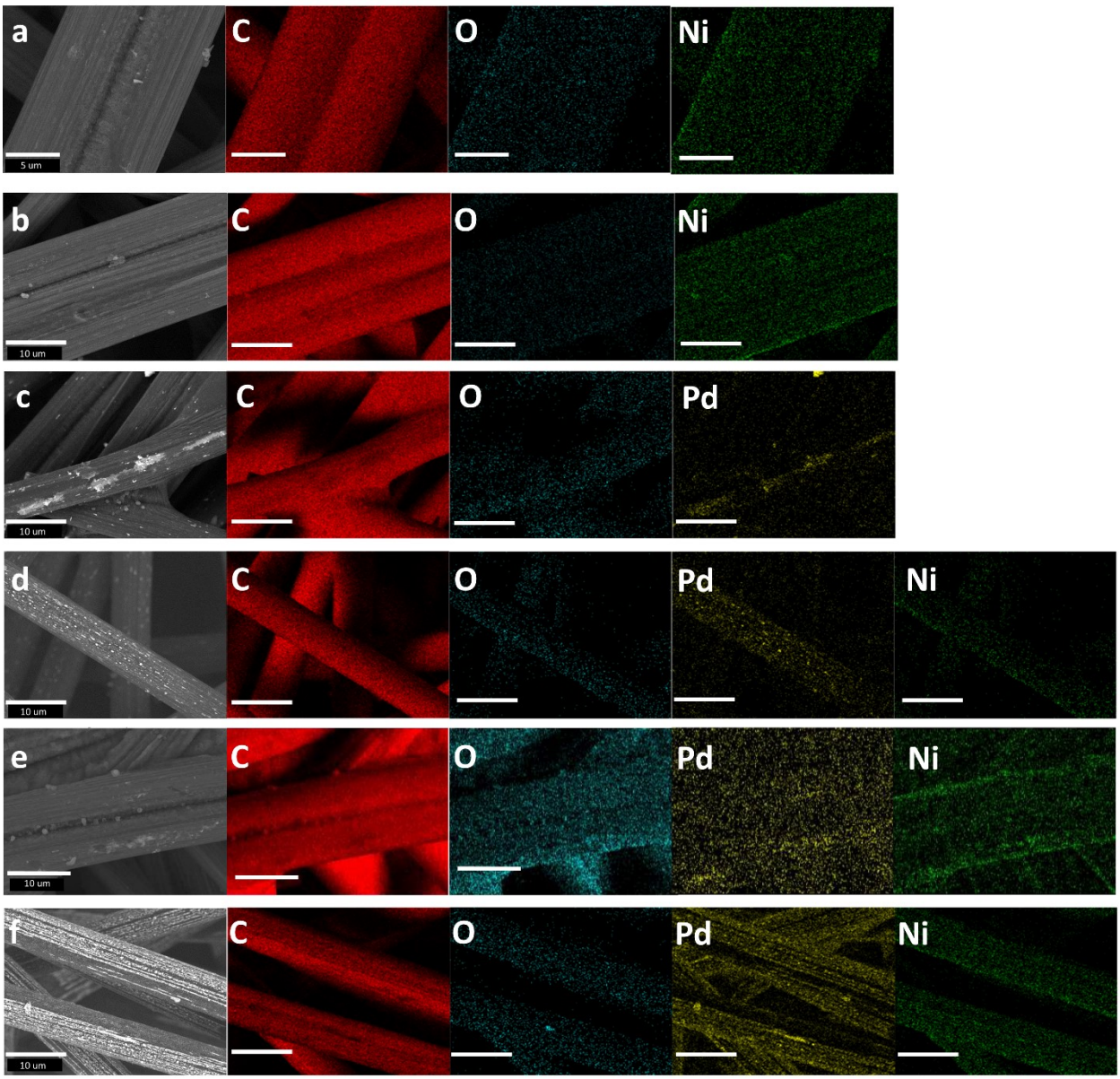

Figure S3. SEM-EDX mapping of: a) GDE-NiO1000, b) GDE-NiO1000-TT, c) GDE-Pd/NiO250, d) GDE-Pd/NiO250-TT, e) GDE-Pd/NiO1000 and f) GDE-Pd/NiO1000-TT.

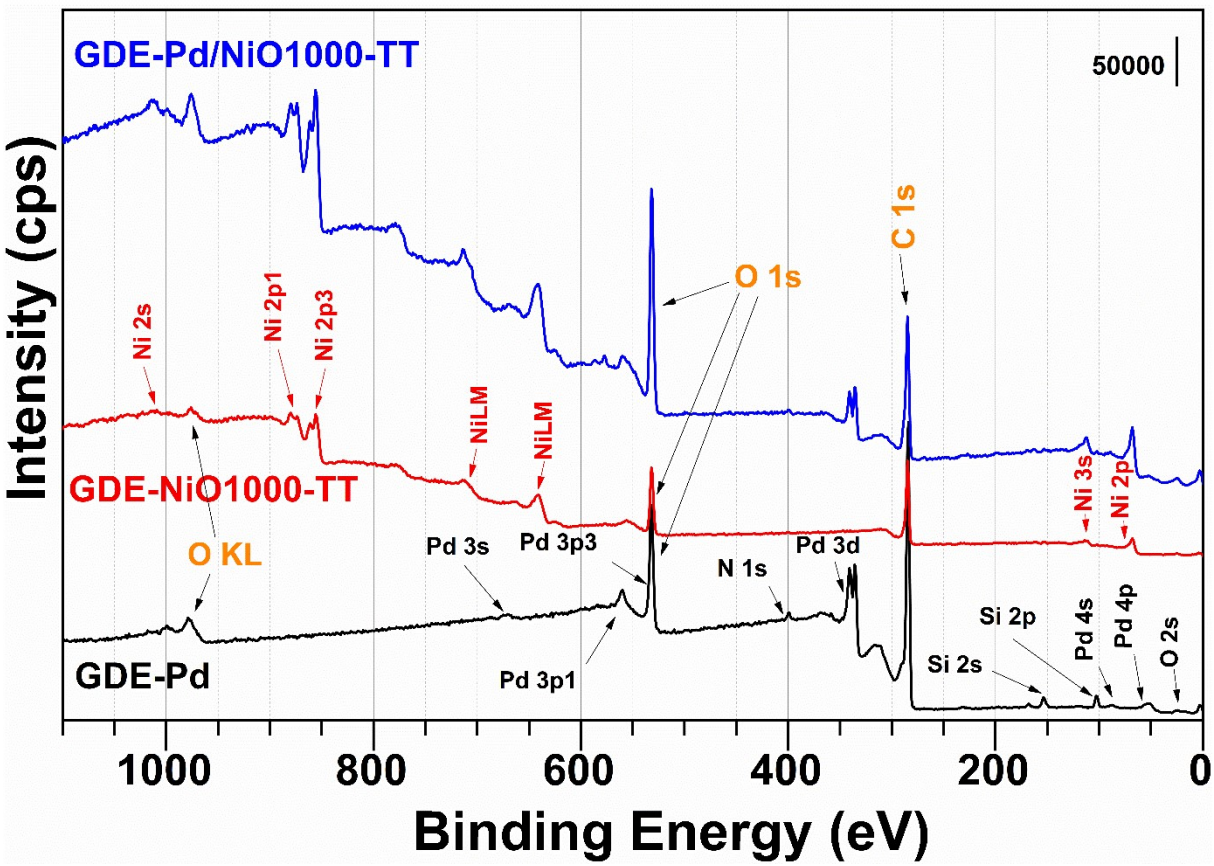

Figure S4: Representative survey XPS spectra of the as-synthesized GDE-Pd, GDE-NiO1000-TT and GDE-Pd/NiO1000-TT electrodes.

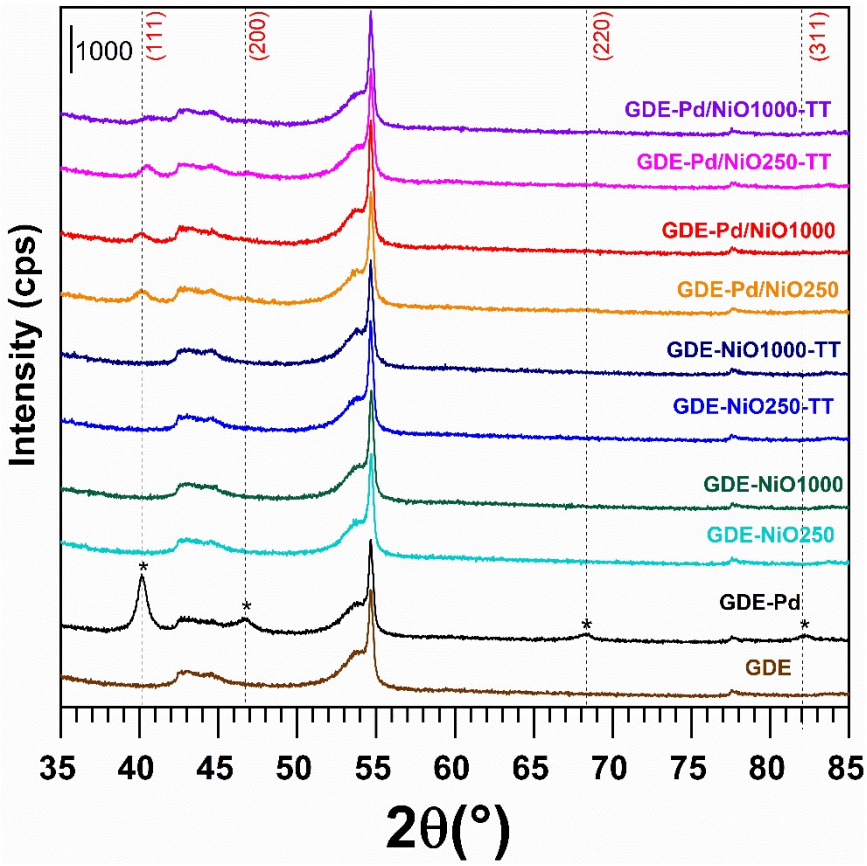

Figure S5: Representative XRD spectra of the as-synthesized GDE-Pd, GDE-NiOX and DGE-Pd/NiOX Electrodes

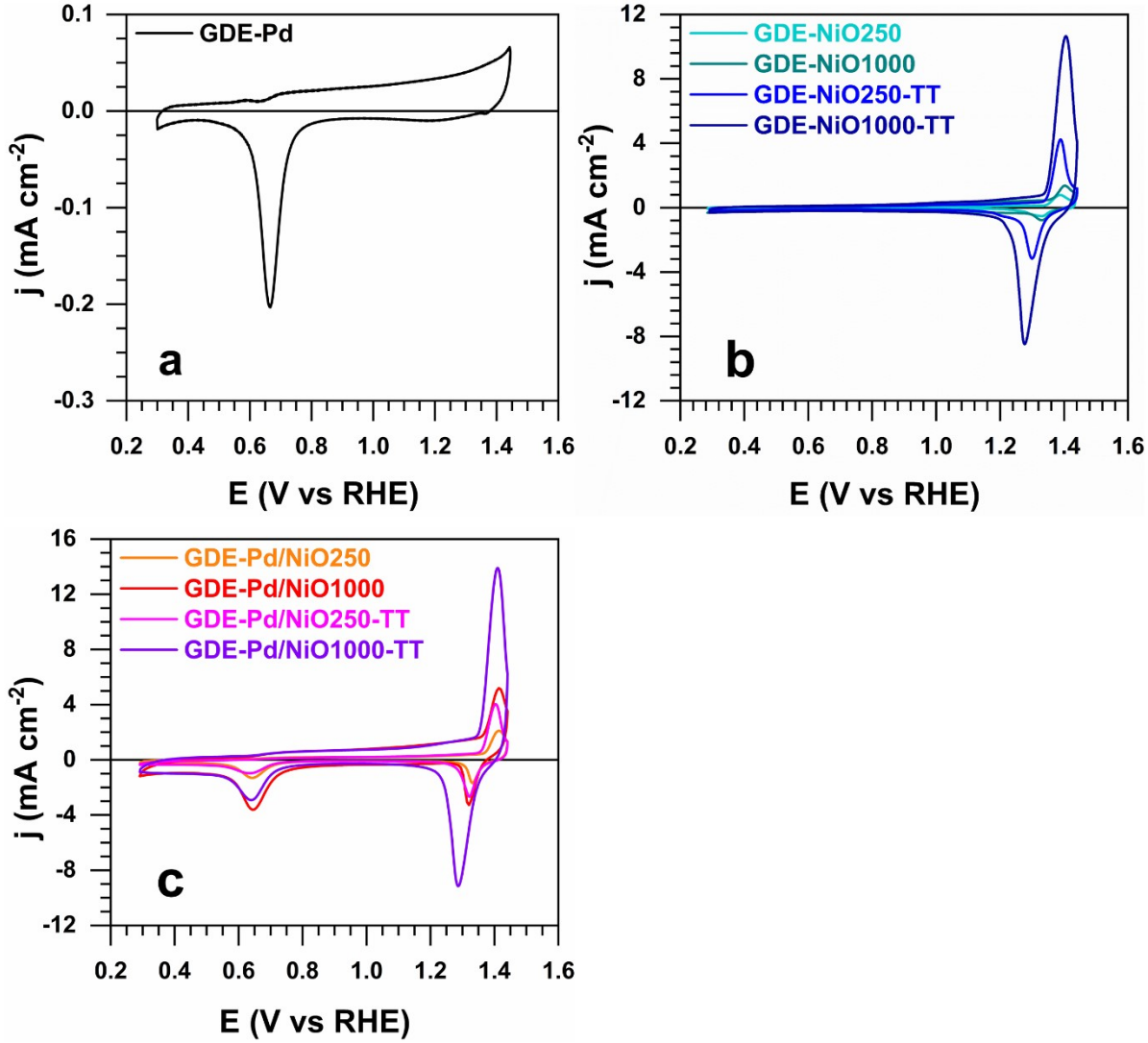

Figure S6: Cyclic voltammetry of various electrocatalysts during the activation process at 100 mV s^{-1} in 1 M KOH at 25 °C.

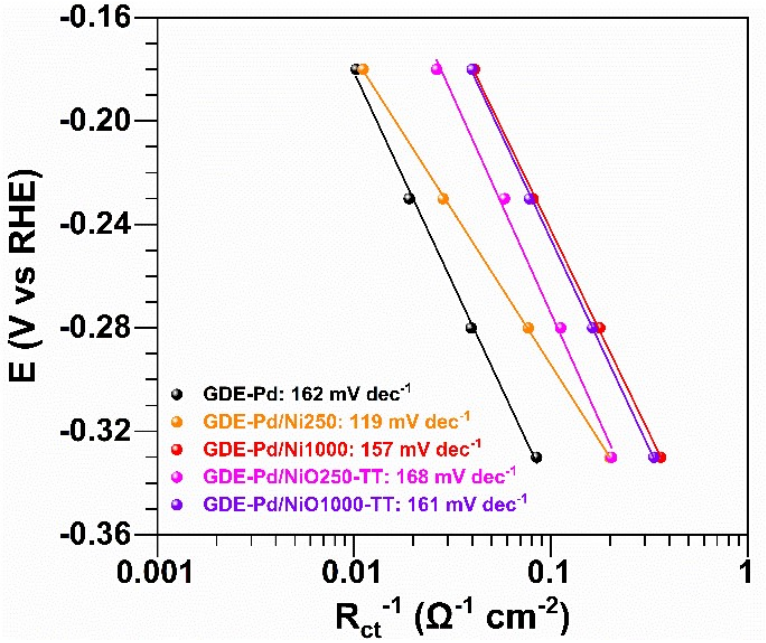

Figure S7: HER: Rct-based Tafel plots from EIS (1 M KOH, 25 °C) of GDE-Pd/NiOX.

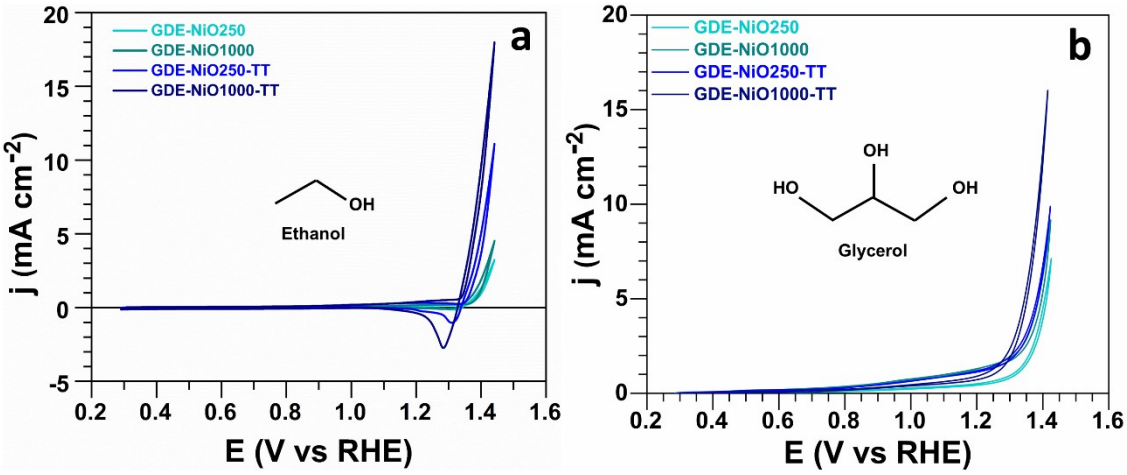

Figure S8: Electrochemical performance of the Ni-based electrodes: a) CV for EtOR (50 mV s^{-1}, 1 M ethanol, 1 M KOH, 25 °C) and b) CV for GOR (50 mV s^{-1}, 1 M glycerol, 1 M KOH, 25 °C).

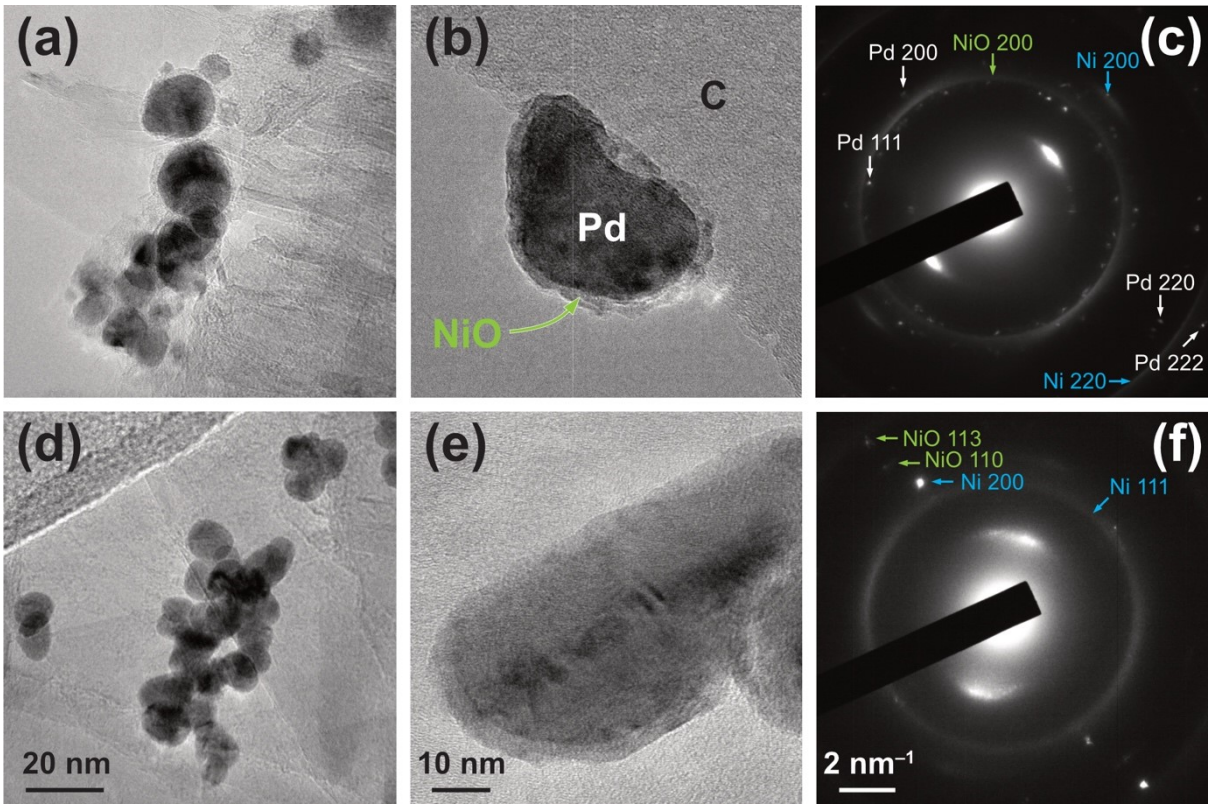

Figure S9: TEM images of Pd/NiO particles on carbon paper (GDE-Pd/NiO1000-TT) before (a,b) and after (d,e) HER at low and high magnification. Corresponding SAED before (c) and after (f) HER.

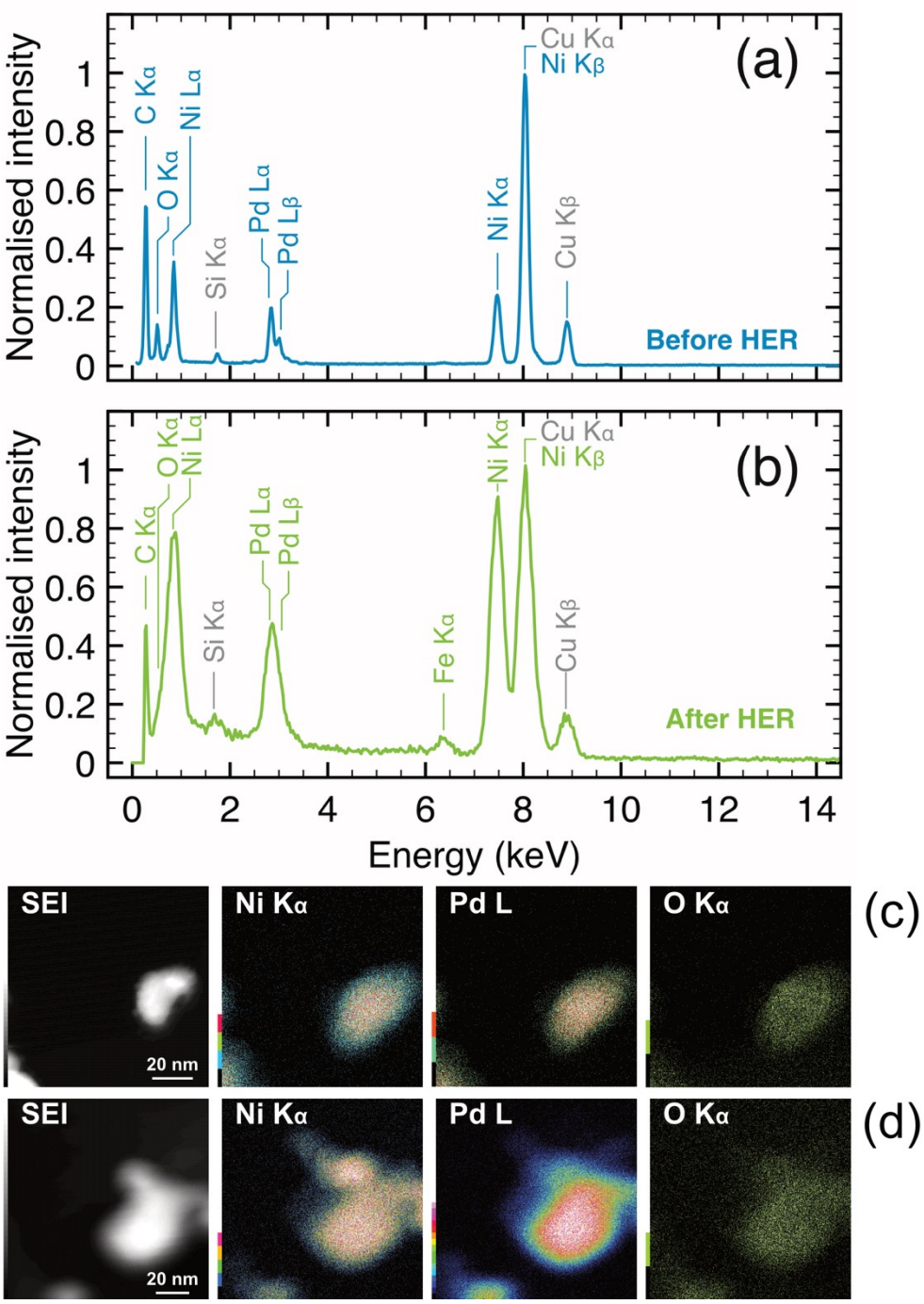
(a)
Normalised intensity
C Kα
O Kα
Ni Lα
Si Kα
Pd Lα
Pd Lβ
Ni Kα
Cu Kα
Ni Kβ
Cu Kβ
Before HER
(b)
Fe Kα
After HER
Energy (keV)
SEI
Ni Kα
Pd L
O Kα
20 nm
(c)
(d)

Figure S10: EDS spectra of Pd/NiO particles on carbon paper(GDE-Pd/NiO1000-TT) before (a) and after (b) HER. EDS mapping of Pd/NiO particles before (c) and after (d).

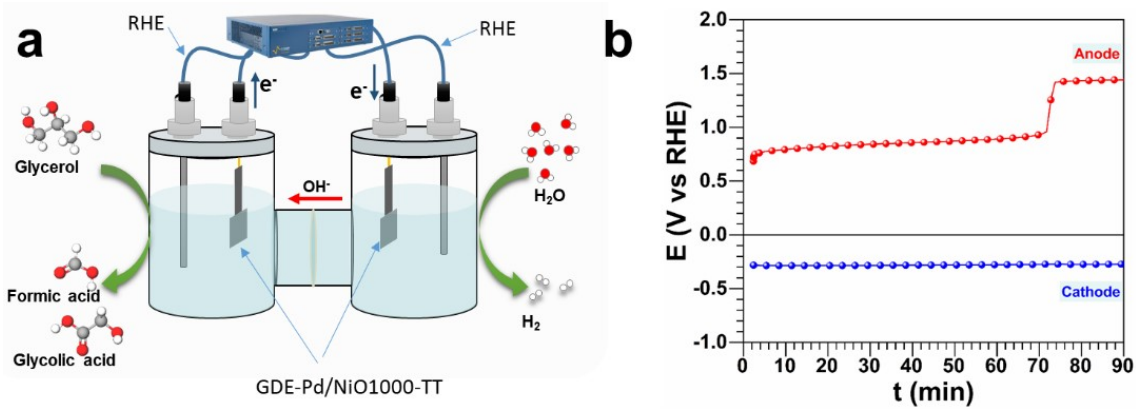

Figure S11. (a) Experimental set-up of H-type cell for the bulk-electrolysis (temperature: 25 °C, catholyte: 1 M KOH, anolyte: 1 M KOH + 1 M glycerol, hydroxide anion exchange membrane: Sustainion® X37-50 grade RT). (b) Potentials of the anode and the cathode recorded during the galvanostatic operation at an applied current $|I_{applied}|$ of 20 mA (corresponding to a current density $|j_{applied}|$ of 10 mA cm^{-2}): first 1.5 h (the full range is reported in the main text, Figure .

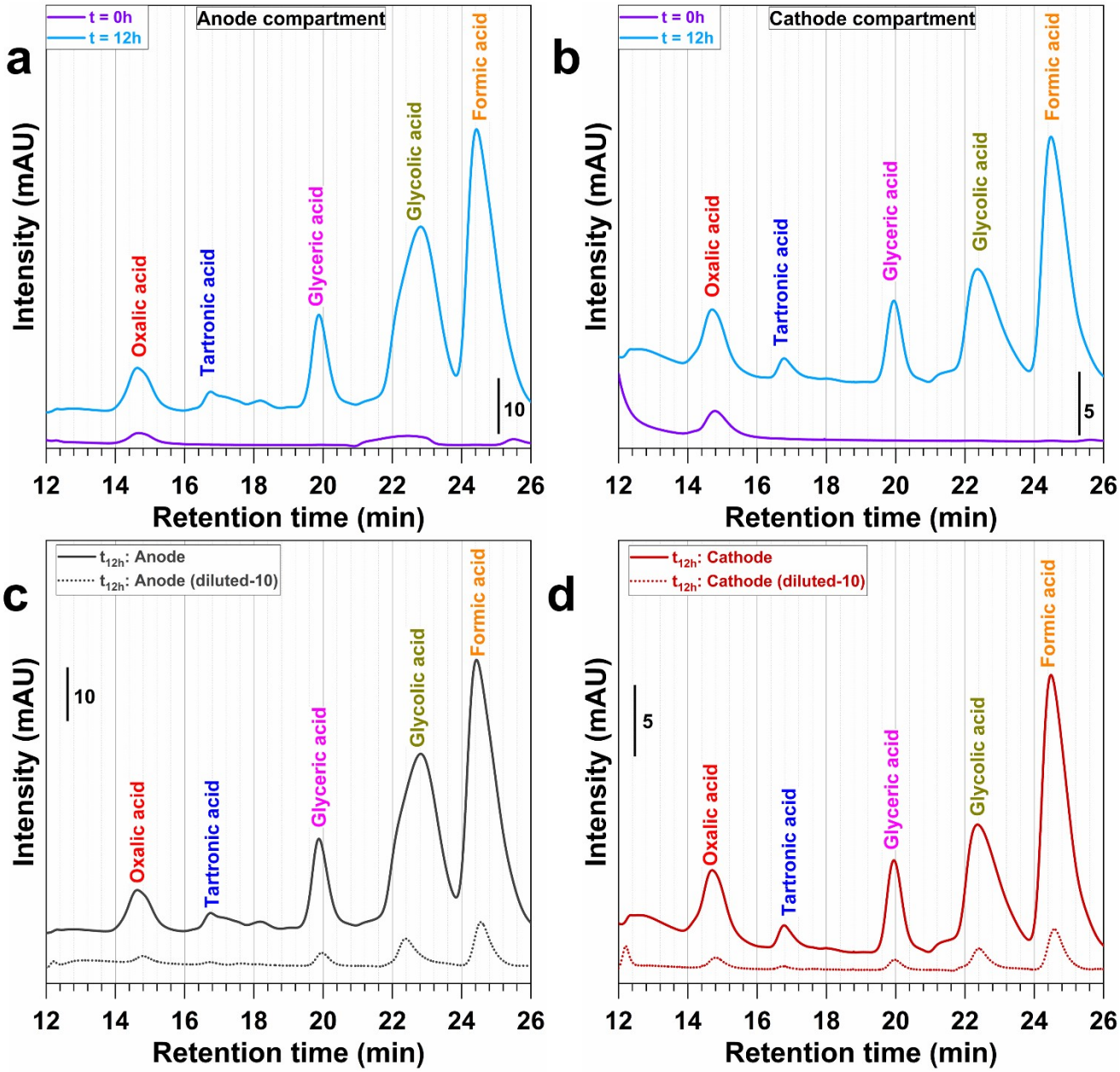

Figure S12: The products distribution chromatograms obtained by HPLC of electrolyte sample taken after glycerol oxidation reaction (GOR) in H-type cell. The example corresponds to a sample taken after 12 hours electrolysis performed at 20 mA for CP, in 1 M KOH containing initially 1 M glycerol. Please note that the intensity for the cathode compartment is twofold (see Y-axis scale bar): the evaluated crossover, that is, $n_{(cathode)}/[n_{(anode)} + n_{(cathode)}]$, is 22-30% depending on the nature of the compound.

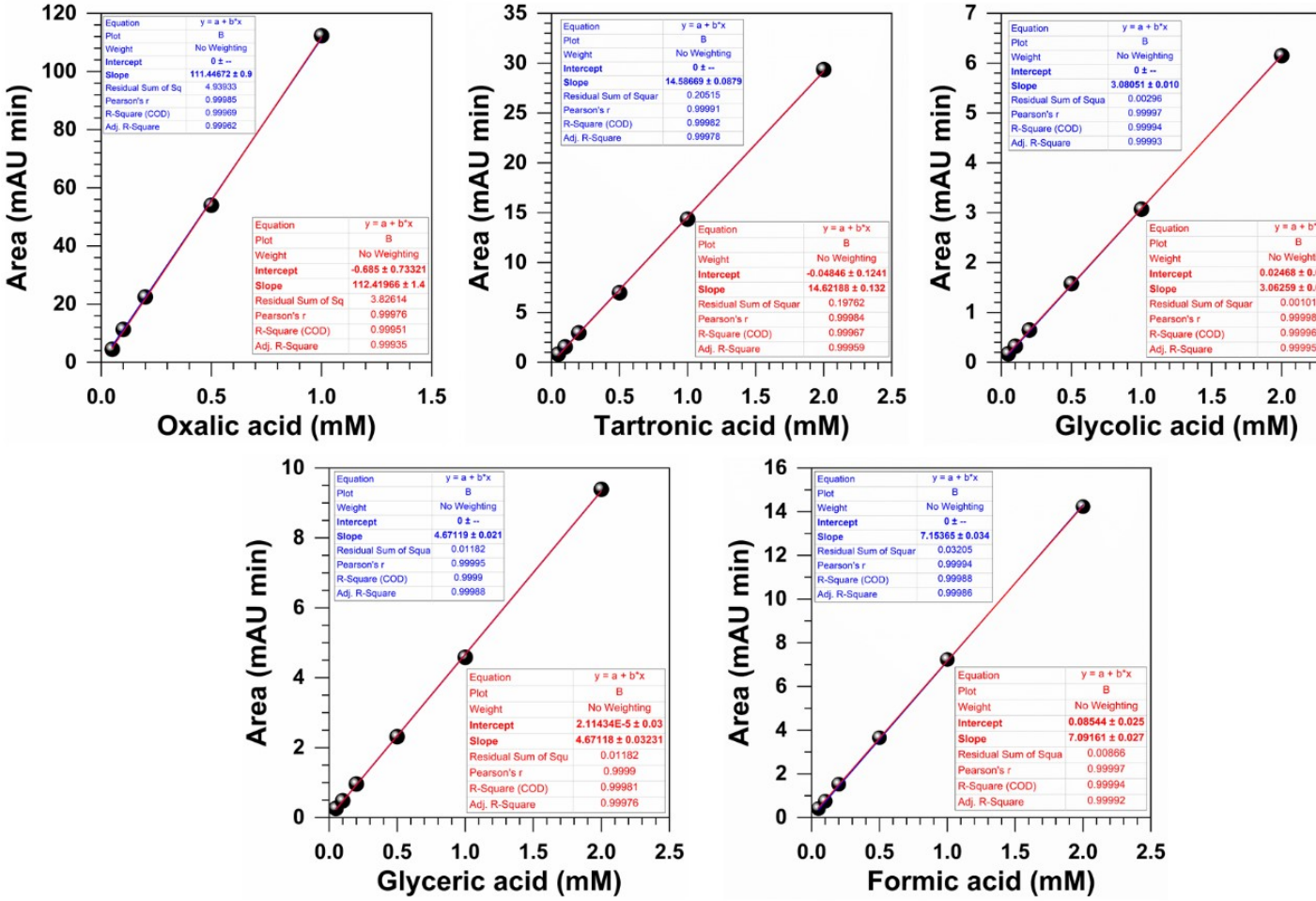

Figure S13: Calibration curves for expected standard reactants.

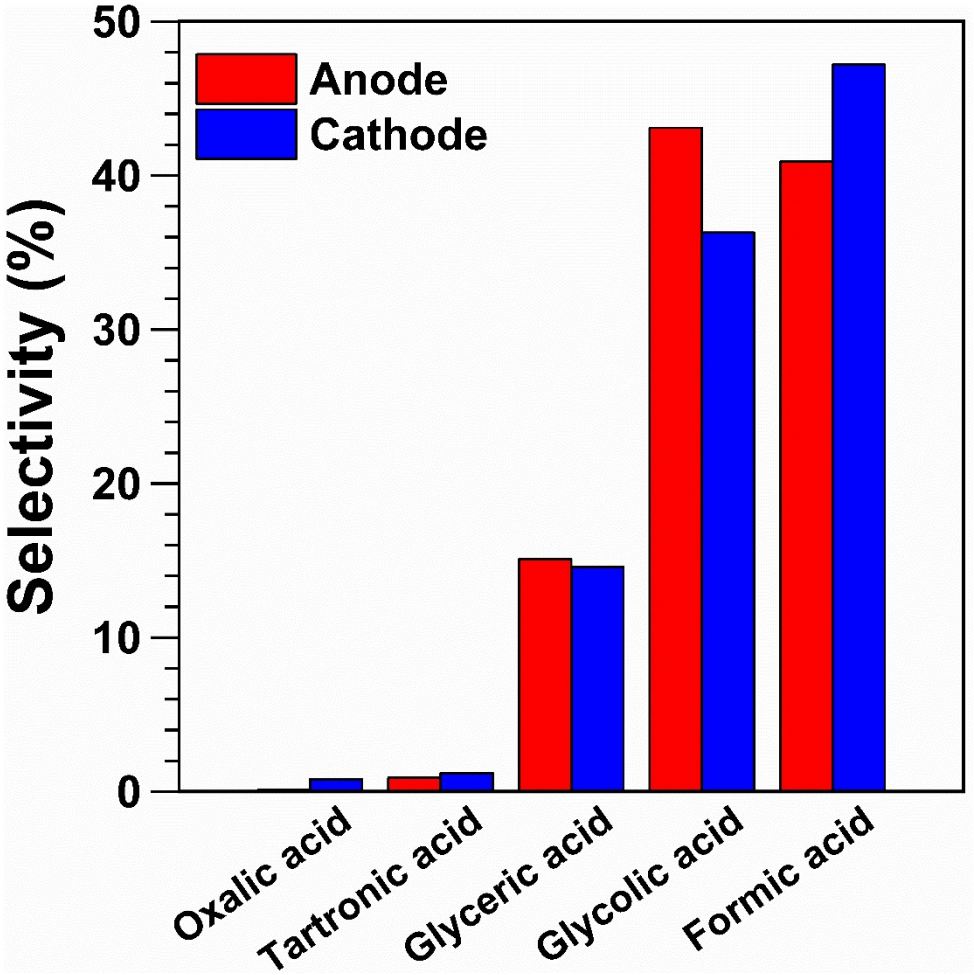

Figure S14: The products distribution relative bar charts from HPLC analysis after GOR in H-type cell.

Note: the evaluated crossover, that is, $n_{(cathode)}/[n_{(anode)} + n_{(cathode)}]$, is 22-30% depending on the nature of the compound, so the products are mainly situated in the anodic compartment.

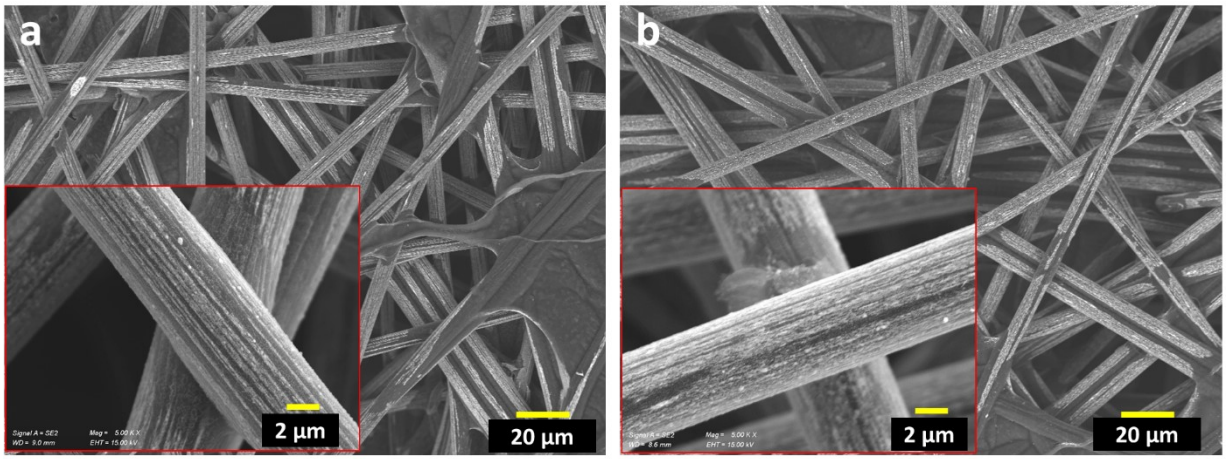

Figure S15. Post-mortem SEM of GDE-Pd/NiO1000-TT 12 hours glycerol electrooxidation in H-type cell: a) anode and b) cathode.

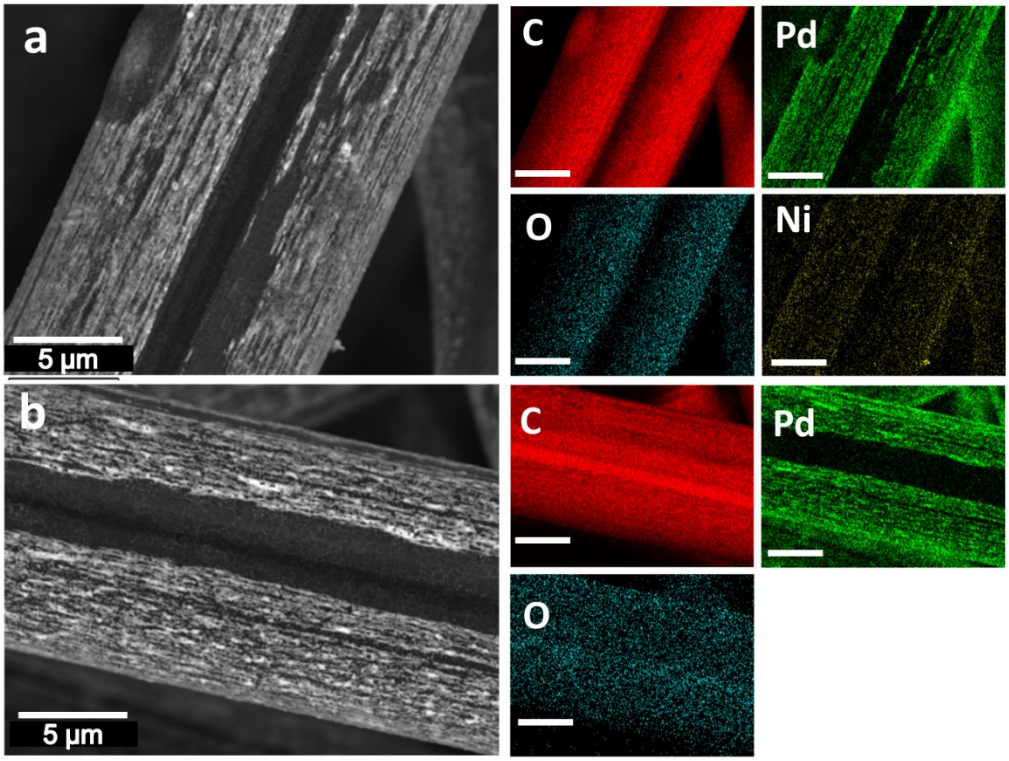

Figure S16. Post-mortem SEM-EDX mapping of GDE-Pd/NiO1000-TT 12 hours glycerol electrooxidation in H-type cell: a) anode and b) cathode.

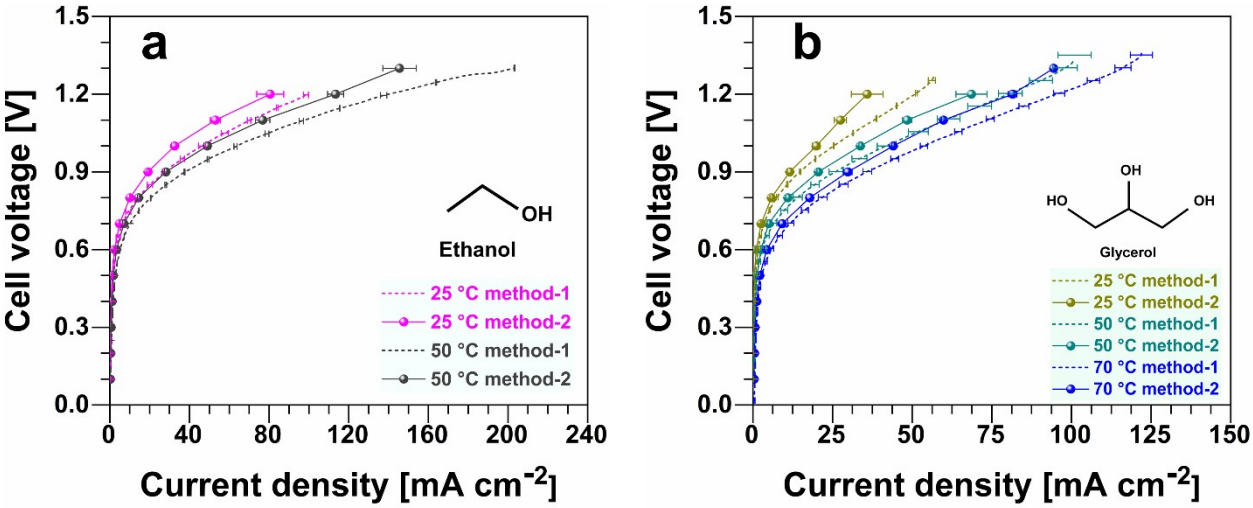

Figure S17. Polarization curves with error bars for GDE-Pd/NiO1000-TT ‖ GDE-Pd/NiO1000-TT Zero-gap biomass-fed electrolyzer using both the potentiostatic method (0.1 V step, method-1) and galvanostatic method (0.05 V s–1 scan rate, method-2): a) for ethanol-fed electrolyzer, b) for glycerol-fed electrolyzer, highlighting performance under each method. Catholyte: 1 M KOH (45 mL min−1, 50 °C). Anolyte: 1 M KOH + 1 M ethanol or 1 M glycerol (23 mL min−1, 50 °C). Hydroxide anion exchange membrane: Sustainion® X37-50 grade RT (5 cm^2).

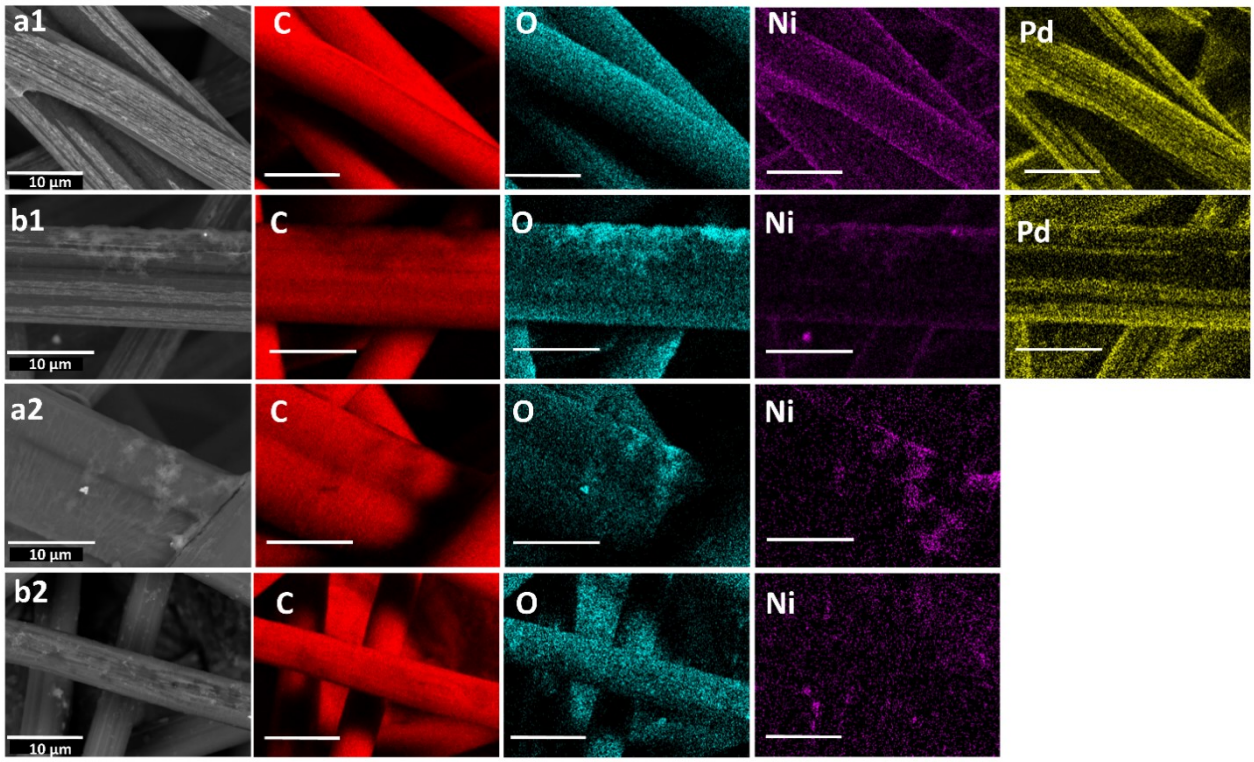

Figure S18. Post-mortem SEM-EDX mapping of GDE-Pd/NiO1000-TT: a1) anode, a2) cathode electrodes from the glycerol-fed electrolyzer, b1) anode a2) cathode electrode from the ethanol-fed electrolyzer.

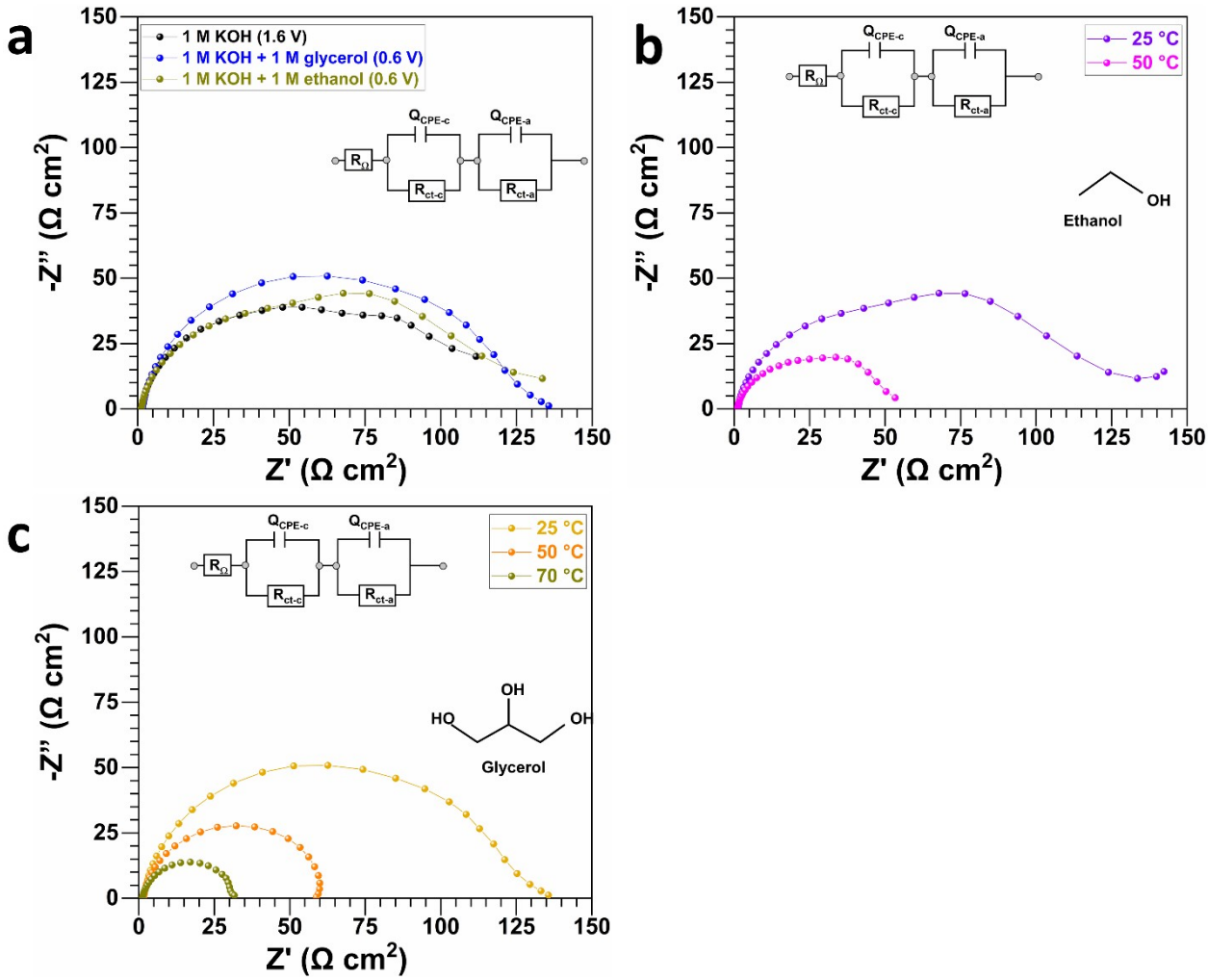

Figure S19. a) Complex-plane Nyquist impedance plots recorded at different cell voltages in the absence and presence of biomass b) recorded at 0.6 V at different temperatures in the ethanol-fed electrolyzer and c) glycerol-fed electrolyzer: inset is the EEC of R_{Ω}+$Q_{\text{CPE-a}}$//$R_{\text{ct-a}}$+$Q_{\text{CPE-c}}$//$R_{\text{ct-c}}$. Catholyte: 1 M KOH (45 mL min^{-1}) and GDE-Pd/NiO1000-TT. Anolyte: 1 M KOH + 1 M ethanol or glycerol (23 mL min^{-1}, 50 °C) and GDE-Pd/NiO1000-TT. Hydroxide anion exchange membrane: Sustainion® X37-50 grade RT (5 cm^2).

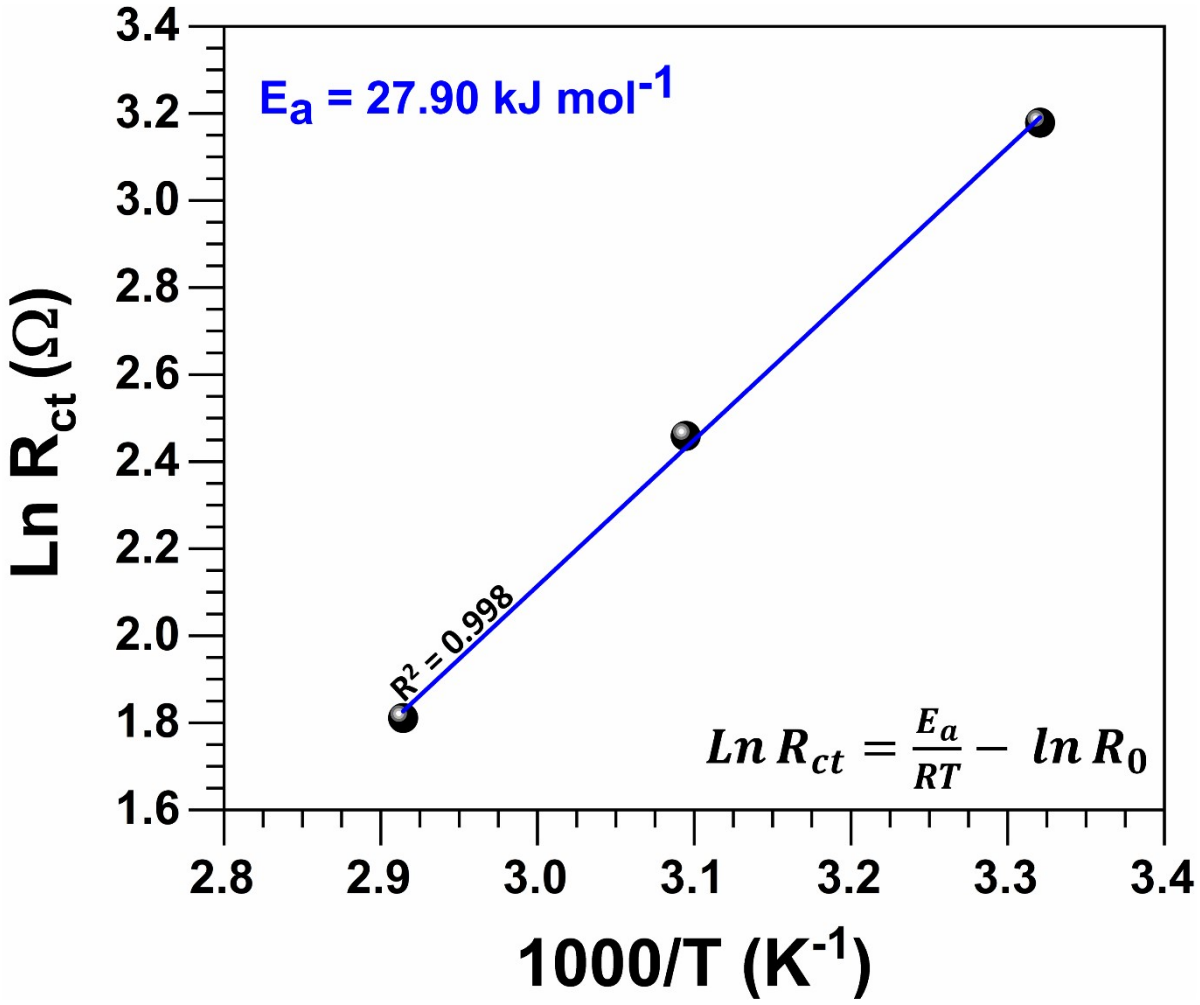

Figures S20: Arrhenius plot for the charge transfer (R_{ct}) resistances for the GDE-Pd/NiO1000-TT electrode.

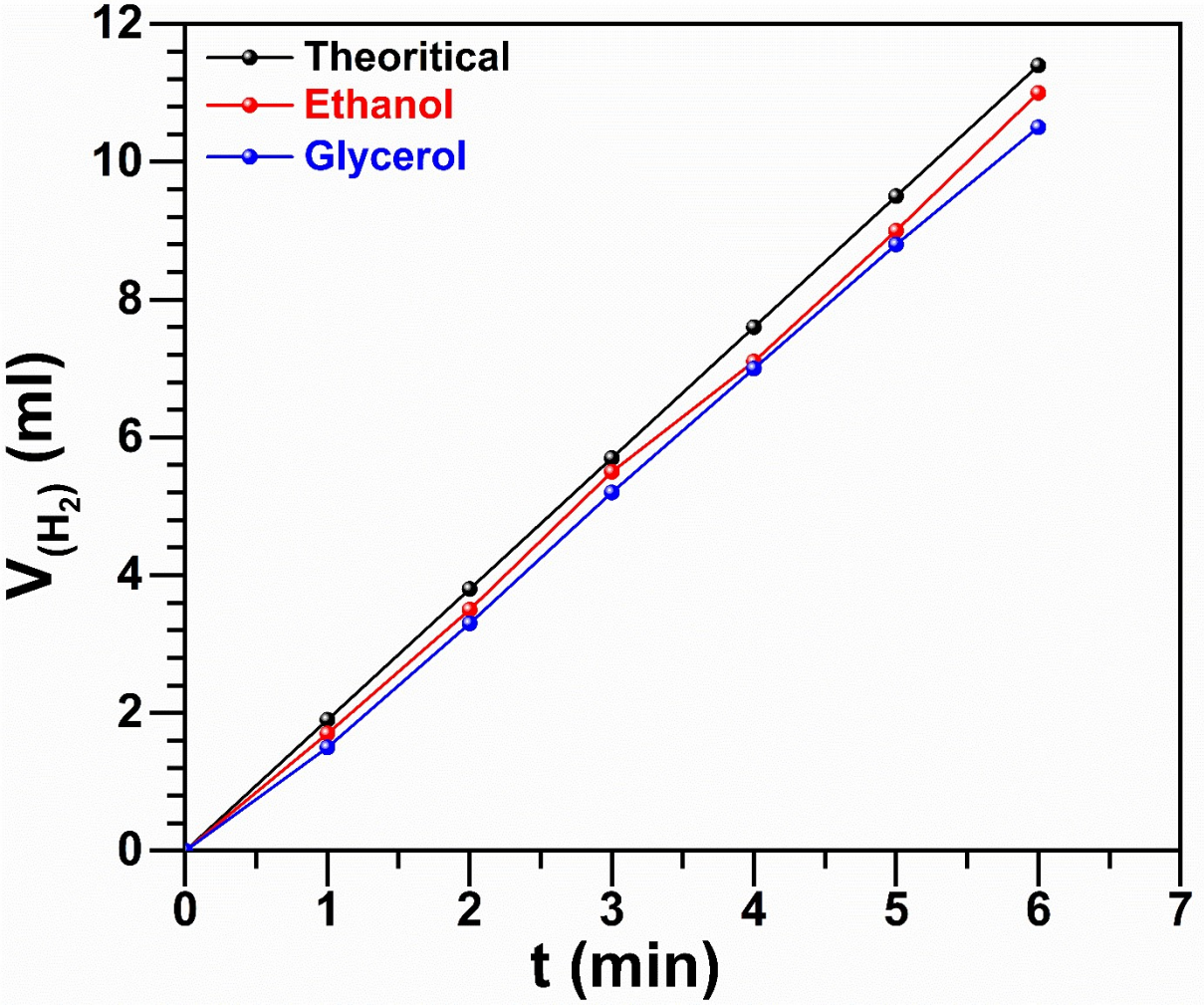

Figures S21: Comparison of hydrogen flow rate from electrolyzer cathodic outlet to theoretical production rates at a current density of 50 mA cm^{-2} (0.25 A).

Table S1. Atomic ratio determined from EDX analysis.

Entry	Atomic %			
	C	O	Ni	Pd
GDE-NiO250	98.7 ± 0.1	1.2 ± 0.1	0.1	-
GDE-NiO250-TT	98.9 ± 0.1	1.0 ± 0.1	0.1	-
GDE-NiO1000	96.7 ± 0.1	2.6 ± 0.1	0.7	-
GDE-NiO1000-TT	98.2 ± 0.2	1.1 ± 0.1	0.7 ± 0.1	-
GDE-Pd/NiO250	98.8 ± 0.1	0.8 ± 0.1	0.1[a]	0.3
GDE-Pd/NiO250-TT	99.0	0.7	0.2	0.1
GDE-Pd/NiO1000	94.2 ± 0.2	4.0 ± 0.2	1.5 ± 0.1	0.3 ± 0.1
GDE-Pd/NiO1000-TT	99.0 ± 0.1	0.6 ± 0.1	0.2	0.2

[a]SD < 0.1

Table S2. Quantitative Data from ICP-OES Analysis.

Entry	ICP-OES					Calculations							
	Used (mg)	Metal (wt%)		%RSD		Metal (μg)		carbon (mg)	GDE(cm²)		Loading (μg cm^{-2}): single face		
		Pd	Ni	Pd	Ni	Pd	Ni		both faces	single face	Pd	Ni	Pd+Ni
GDE-Pd	31.3	0.7	0.0	0.5	0.0	222.2	0.0	31.1	6.8	3.4	32.5	0.0	32.5
GDE-Pd/NiO250-TT	29.6	0.4	0.1	0.3	0.5	112.5	18.4	29.5	6.5	3.2	17.3	5.7	23.0
GDEPd/NiO1000-TT	28.6	0.4	0.3	2.6	0.5	113.8	88.9	28.4	6.2	3.1	18.2	28.5	46.7
GDE_Pd/NiO1000	37.7	0.4	0.3	0.7	0.5	159.1	108.2	37.4	8.2	4.1	19.3	26.3	45.6
GDE_NiO1000	22.1	0.0	0.0	0.0	0.4	0.0	4.2	22.1	4.9	2.4	0.0	1.7	1.7

Table S3. Fitted EIS Data for HER in 1 M KOH at 25 °C and corresponding LSV details. The applied potential is iR-drop uncorrected.

Entry	$E_{applied}$ (mV vs RHE)	Cell resistance R_s(Ω cm^2)	Charge transfer resistance R_{ct}(Ω cm^2)	η@-10 mA/cm^2(V)
GDE-Pd	-174	1.9	151.2	0.40
GDE-NiO250	-174	1.7	711	0.51
GDE-NiO250-TT	-174	1.8	459.2	0.47
GDE-NiO1000	-174	2.0	1204.5	0.47
GDE-NiO1000-TT	-174	3.3	152.4	0.38
GDE-Pd/NiO250	-174	2.1	90.2	0.32
GDE-Pd/NiO250-TT	-174	2.1	39.1	0.29
GDE-Pd/NiO1000	-174	2.2	24.5	0.27
GDE-Pd/NiO1000-TT	-174	1.9	25.1	0.26

Table S4. ECSA values and GOR comparative data for various electrocatalysts.

Electrocatalyst	$ECSA_{PdO}$ (cm^2)	E_{onset} (V vs RHE)	$E_{@10\ mA/cm^2}$ (V vs RHE)	j_p (mA cm^{-2})	j_p (mA $cm^{-2}{}_{ECSA}$)
GDE-Pd	0.35	0.42	0.86	11.1	15.9
GDE-Pd/NiO250	2.6	0.38	0.80	12.6	2.4
GDE-Pd/NiO250-TT	3.1	0.35	0.79	19.2	3.1
GDE-Pd/NiO1000	5.2	0.32	0.77	38.8	3.7
GDE-Pd/NiO1000-TT	13.2	0.30	0.72	79.0	3.0

Table S5. Fitted EIS data for glycerol oxidation in 1 M KOH + 1 M glycerol at 25 °C and corresponding CV details. The applied potential is iR-uncorrected.

Entry	$E_{applied}$ (V vs RHE)	Cell resistance R_s(Ω cm^2)	Charge transfer resistance R_{ct}(Ω cm^2)	E_{onset}(V vs RHE)
GDE-Pd	0.67	3.4	134.2	0.42
GDE-Pd/NiO250	0.67	2.6	51.8	0.38
GDE-Pd/NiO250-TT	0.67	3.4	57.5	0.35
GDE-Pd/NiO1000	0.67	2.5	33.0	0.32
GDE-Pd/NiO1000-TT	0.67	2.5	16.6	0.30

Table S6. Quantitative Data from ICP-OES Analysis after 68 h HER operation.

Initially, the metal content within the GDE-Pd/NiO1000-TT electrode is 18.2 µg(Pd) cm^{-2} and 28.5 µg(Ni) cm^{-2}. Used electrode area: 1 cm^2. The completed dissolution would lead to '18.2 µg of Pd in 40 mL solution' and '28.5 µg of Ni in 40 mL solution', so, 910 µg(Pd) L^{-1} and 1425 µg(Ni) L^{-1}.

Entry	**ICP-OES**			
	Metal content in µg L^{-1}, i.e. ppb (cumulative dissolved mass in µg)		RSD (%)[b]	
	Pd	Ni	Pd	Ni
Electrolyte: 20 h	< 10[a]	8 (0.3)	-	5
Electrolyte: 29 h	< 10[a]	13 (0.8)	-	3
Electrolyte: 42 h	< 10[a]	14 (1.4)	-	7
Electrolyte: 53 h	< 10[a]	17 (2.1)	-	4
Electrolyte: 68 h	< 10[a]	11 (2.5)[c]		2

[a] Not quantified because results are below the lowest point of the calibration and below the detection limit
[b] RSD: Relative Standard Deviation
[c] This means that the total dissolved nickel is 2.5 µg, out of 2

Table S7. Fitted EIS data of the electrolysis cell by R_{Ω}+Q_{CPE}//$R_{ct\text{-}a}$+Q_{CPE}//$R_{ct\text{-}c}$: effect of temperature. Catholyte: 1 M KOH (45 mL min^{-1}). Anolyte: 1 M KOH + 1 M glycerol (23 mL min^{-1}). Hydroxide anion exchange membrane: Sustainion® X37-50 grade RT (5 cm^2).

Temperature (°C)	$U_{applied}$ [V]	R_{Ω} [Ω cm^2]	Anode			Cathode		
			$R_{ct\text{-}a}$ [Ω cm^2]	$Q_{CPE\text{-}a}$ [mF s$^{(a-1)}$]	a	$R_{ct\text{-}c}$ [Ω cm^2]	$Q_{CPE\text{-}c}$ [mF s$^{(a-1)}$]	a
25	0.6	1.2	120.1	4.66	0.9	3.16	89.55	0.3
50	0.6	1.2	58.5	4.29	0.9	0.68	59.48	0.6
70	0.6	1.0	30.6	4.64	0.9	0.30	27.1	0.8

Table 8. Fitted EIS data of the electrolysis cell by R_{Ω} +Q_{CPE}//$R_{ct\text{-}a}$+Q_{CPE}//$R_{ct\text{-}c}$: effect of temperature. Catholyte: 1 M KOH (45 mL min^{-1}). Anolyte: 1 M KOH + 1 M ethanol (23 mL min^{-1}). Hydroxide anion exchange membrane: Sustainion® X37-50 grade RT (5 cm^2).

Temperature (°C)	$U_{applied}$ [V]	R_{Ω} [Ω cm^2]	Anode			Cathode		
			$R_{ct\text{-}a}$ [Ω cm^2]	$Q_{CPE\text{-}a}$ [mF s$^{(a-1)}$]	a	$R_{ct\text{-}c}$ [Ω cm^2]	$Q_{CPE\text{-}c}$ [mF s$^{(a-1)}$]	a
25	0.6	1.0	77.8	6.69	0.91	0.15	1.81	1
50	0.6	0.9	40.11	7.32	0.90	0.09	2.82	1

Table S9. Comparison of the performance of relevant metallic catalysts for the hydrogen evolution reaction in alkaline media from literature.
The metal loading is normalized to the geometric area. WE: working electrode. C: carbon black Vulcan. HSAG: high surface area graphite. *L*: metal loading on the electrode (total), per square centimeter of the electrode. *T*°: temperature. RT: room temperature. GC: glassy carbon. GDE: gas diffusion electrode. CWM: carbonized wood membrane. Empty box (–) means that the original article does not provide the data.

Ref.	Electrode material			Conditions		Performance	
	Nanocatalyst (metal loading)	WE (area)	*L* (mg cm^{-2})	Electrolyte	T° (°C)	η @-10 mA cm^{-2} (mV)	Tafel slope (mV dec^{-1})
Herein	GDE-Pd	GDE	0.03	1 M KOH	25	400	162
	GDE-Pd/NiO1000		0.02			270	168
	GDE-Pd/NiO1000-TT		0.02			260	161
2024 [1]	MoO_x/Pd	FTO	1.4	0.1 M KOH	-	107	502
2022 [2]	Pd@MoS_2/$Mo_2TiC_2T_x$	GC	2.55	1.0 M KOH	25	100	80
2021 [3]	Pd NPs	CWM	3.89	1.0 M KOH	-	302	64.5
2020 [4]	Pd–P/Pt–Ni NPs	GC	28.5	1.0 M KOH	25	21	55.4
2020 [5]	Cu-Pd	HSAG	-	0.1 M KOH	RT	145	75
2018 [6]	Mesoporous Pd@Ru NRs	GCE	0.05	1.0 M KOH	RT	30	30
	Solid Pd@Ru NRs	GCE	0.05	1.0 M KOH	RT	76	48
2016 [7]	Ni_3N/Pt	Ni mesh	2	1.0 M KOH	-	50	36.5
2015 [8]	$Ni_{0.33}Co_{0.67}S_2$ NWs	bare Ti	0.3	1.0 M KOH	RT	88	118

Table S10. Comparison of the performance of relevant metallic catalysts for the glycerol electrooxidation reaction in alkaline media from literature.
The metal loading is normalized to the geometric area. WE: working electrode. C: carbon black Vulcan. *L*: metal loading on the electrode (total), per square centimeter of the electrode. Gly.: glycerol. *T*°: temperature. RT: room temperature. E_{onset}: onset potential. j_p: peak current density and expressed in either amps per milligram of metal (A mg^{-1}) or milliamps per square centimeter of the electrode (mA cm^{-2}). GC: glassy carbon. GDE: gas diffusion electrode. Empty box (–) means that the original article does not provide the data.

Ref.	Electrode material			Conditions		Performance (50 mV s^{-1} at scan rate)		
	Nanocatalyst (metal loading)	WE (area)	*L* (μg cm^{-2})	Electrolyte + Glyc.	T° (°C)	E_{onset} (V vs RHE)	j_P (A mg^{-1})	j_P (mA cm^{-2})
Herein	GDE-Pd	GDE (0.5 cm^{-2})	32	1 M KOH + 0.1 M Glyc.	25	0.42	0.3	11.2
	GDE-Pd/NiO1000		19			0.32	1.9	36.8
	GDE-Pd/NiO1000-TT		18			0.3	4.3	79.0
ACS Appl. Energy Mater. 2024, 7, 5, 1802–1813.[9]	PdNi/C	GDE	299	1 M NaOH + 0.5 M Glyc.	25	0.6	0.211	2.2
	Pd/C		500			0.6	0.17	1.3
ACS Appl. Energy Mater. (2021) 4 (9), 9944-9960.[10]	$Pd_{0.8}Fe_{0.2}$/rGO (19.0 wt%)	GC (0.196 cm^2)	38.7	1 M KOH + 1 Glyc.	25	0.50	1.9	59.0
				1 M KOH + 0.1 M Glyc.		0.52	1.1	35.2
	$Pd_{0.8}Fe_{0.2}$/Vulcan (19.0 wt%)		38.7			0.52	0.8	24.4
	Pd/rGO (19.8 wt%)		40.3			0.52	0.5	21.4
	Pd/Vulcan (19.5 wt%)		39.7			0.52	0.6	23.7
	Pd/C (20 wt%, commercial)		47.9			0.58	0.4	18.9
J. Catal. 377 (2019) 358-366.[11]	Ir-Pd nanocubes	GC (0.8 cm^2)	6.25	1 M NaOH + 1 M Glyc.	–	0.6	*[16 mA cm^{-2}]/6.25 μg_{Pt} cm^{-2}]=2.5*	16
ChemElectroChem, 2018, 5, 743-747.[12]	ACF-Pd (1 wt.%): ~1 cm^2		96	0.1 M KOH + 0.1 M Glyc.	RT	<0.5	0.44	40

Chem. Commun., 2017, 53, 1642-1645.[13]	Pd nanosheets	GC (0.07 cm^2)	137	1 M NaOH + 0.1 M Glyc.	RT	0.50	0.55	70
J. Power Sources 351 (2017) 174-182.[14]	Ni@Pt/MWCNTs (40 wt%)	GC (0.07 cm^2)	320	1 M NaOH + 0.5 M Glyc.	–	0.49	0.27	79
Chem. Eng. J. 308 (2017) 419-427.[15]	Pd-NiOx-P/C (20 wt.%)	GC (0.196 cm^2)	8	0.1 M KOH + 0.5 M Glyc.	25	0.5	0.36	$[8\ \mu g_{Pt}\ cm^{-2}]*[0.36\ mA\ \mu g^{-1}_{Pt}] = 2.88$
ChemElectroChem, 2016, 3, 1694-1704.[16]	$Pt_3Pd_6Bi_1/C$ (40 wt.%)	GC (0.07 cm^2)	100	1 M NaOH + 0.1 M Glyc.	RT	0.4	–	40
Energy Environ. Sci., 2016, 9, 3097-3102.[17]	Pd/C nanosponge	GC (0.07 cm^2)	–	1 M KOH + 0.1 M Glyc.	–	0.65	–	15
J. Am. Chem. Soc., 2014, 136, 3937-3945.[18]	Pd sel-supported	GC (0.25 cm^2)	200	1 M KOH + 0.1 M Glyc.	–	0.6	0.1	–
RSC Adv., 2014, 4, 64476-64483.[19]	Pd/C (40 wt.%)	GC (0.07 cm^2)	320	0.1 M KOH + 0.1 Glyc.	–	0.65	0.025	–
ACS Catal., 2013, 3, 2403-2411.[20]	Pd/C (30 wt.%)	GC (0.07 cm^2)	116	0.1 M NaOH + 0.1 M Glyc.	RT	0.50	0.16	–
Electrochem. Commun., 2013, 34, 185-188.[21]	Pd	GC (0.07 cm^2)	200	1 M NaOH + 0.1 M Glyc.	RT	0.63	0.4	–
Appl. Catal. B: Env., 2010, 93, 354-362.[22]	Pd/C (40 wt.%)	GC (0.07 cm^2)	142	1 M KOH + 0.1 M Glyc.	20	0.6	–	25

Table S11. Comparison of the performance of relevant metallic catalysts for the ethanol electrooxidation reaction in alkaline media from literature.

Ref.	Electrode material	Conditions	Performance	
	Nanocatalyst	Electrolyte	j_p (mA mg^{-1})	j_p (mA cm^{-2})
Herein	GDE-Pd	1 M KOH + 1 M EtOH	378	12.31
	GDE-Pd/NiO1000		2745	52.88
	GDE-Pd/NiO1000-TT		3440	62.78
J. Colloid Interface Sci., 2023, 650, 350.[23]	PdPtNi PNSs	1 M KOH + 1 M EtOH	6180	18.84
Appl Catal B Environ, 2021, 280, 119464.1.[24]	Pd/NCB@NGS-2	1 M KOH + 1 M EtOH	2690	-
Nanoscale, 2019, 11, 2974-2980.[25]	PdRh NBs	1 M KOH + 1 M EtOH	630	4.8
Appl. Catal. B: Env., 2019, 249, 116.[26]	Ultrathin Pd_2Ag_1 NWs	1 M KOH + 1 M EtOH	2843	-
Adv. Mater. 2017, 29, 1701331.[27]	Au@Pd Core–Shell Nanorods	1 M KOH + 1 M EtOH	2920	-
J. Power Sources 2016, 301, 160.[28]	Pd3Pb nanoflowers	1 M KOH + 0.5 M EtOH	~510	-
Nanoscale 2015, 7, 12445.[29]	Pd7/Ru1 nanodendrites	1 M KOH + 1 M EtOH	~1150	-
Nanoscale, 2014, 6, 2768.[30]	PdCu nanocapsules	1 M KOH + 1 M EtOH	1140	-
Adv. Mater. 2012, 24, 2326.[31]	10.8-nm-thick PdPt NWs	1 M KOH + 0.5 M EtOH	940	-

Table S12. Performance of relevant data from literature towards glycerol electrolysis in alkaline media. Empty box (–) means that the original article does not provide such data.

Cathode		Separator (temperature)	Anode		Performance	Ref.
Electrocatalyst	Catholyte		Electrocatalyst	Anolyte		
GDE-Pd/NiO1000-TT	1 M KOH	Sustainion® X37-50 grade RT	GDE-Pd/NiO1000-TT	1 M KOH + 1 M EtOH	j_{10}: 0.69 V	Herein
				1 M KOH + 1 M Gly.	j_{10}: 0.67 V	
C@Ni-Pd	1 M KOH + 1 M EtOH	Fumasep FAB-PK-130	C@Ni-Pd	1 M KOH + 1 M EtOH	j_{10}: 0.55 V	Chem. Eng. J., 2023, 474, 145639.[32]
PtCu NF/C	1.0 M KOH	Nafion 211	PtCu NF/C	1 M KOH + 0.5 M EtOH	j_{10}: 0.58 V acetate	ACS Catal. 2022, 12, 18, 11402–11411.[33]
				1 M KOH + 0.5 M Glyc.	j_{10}: 0.68 V NA	
Pt wire	1 M KOH + 1 M EtOH	Nafion-115 proton membrane	$Ni_{0.75}Co_{0.25}Se_2$ NPs	1 M KOH + 1 M EtOH	J_{10}: 1.4 V acetate	Chem. Eng. J. 2022, 440, 135817.[34]
NC/Ni-Mo-N/NF	1 M KOH + 0.1 M Glyc.	Not separated	NC/Ni-Mo-N/NF	1 M KOH + 0.1 M Glyc.	j_{10}: 1.38 Format	Appl. Catal. B, 2021, 298, 120493.[35]
SA In-Pt NWs/C (12.8 μg_{Pt})	1.0 M KOH	Nafion 211	SA In-Pt NWs/C	1 M KOH + 0.5 M EtOH	j_{10}: 0.62 V acetic acid	Adv. Funct. Mater. 2020, 30, 2004310.[36]
				1 M KOH + 0.5 M Glyc.	j_{10}: 0.78 V NA	
Ni-Mo-N/CFC	1 M KOH + 0.1 M Glyc.	Not separated	Ni-Mo-N/CFC	1 M KOH + 0.1 M Glyc.	j_{10}: 1.36 formate	Nat Commun 10, 5335 (2019).[37]
Pt/C	1 M KOH + 15:5 volume ratio of EtOH to water	–	F-modified FeOOH	1 M KOH + 0.33 M EtOH	j_{10}: 1.43 acetic acid	ACS Catal. 2018, 8, 1, 526–530.[38]

References

1 U. K. Ghorui, B. Show, D. Roy, A. Basak, B. Adhikary and A. Mondal, *ACS Appl. Mater. Interfaces*, 2024, **16**, 3460–3475.
2 L.-H. Zheng, C.-K. Tang, Q.-F. Lü and J. Wu, *International Journal of Hydrogen Energy*, 2022, **47**, 11739–11749.
3 W. Deng, Y. Li, F. Wang, Q. Ma and S. Min, *Electrocatalysis*, 2021, **12**, 340–349.
4 Y. Wu, M. Zhao, J.-P. Cao, J. Xu, T. Jin and N. Asao, *Chem. Commun.*, 2020, **56**, 8984–8987.
5 M. Nunes, D. M. Fernandes, M. V. Morales, I. Rodríguez-Ramos, A. Guerrero-Ruiz and C. Freire, *Catalysis Today*, 2020, **357**, 279–290.
6 Y. Luo, X. Luo, G. Wu, Z. Li, G. Wang, B. Jiang, Y. Hu, T. Chao, H. Ju, J. Zhu, Z. Zhuang, Y. Wu, X. Hong and Y. Li, *ACS Appl. Mater. Interfaces*, 2018, **10**, 34147–34152.
7 Y. Wang, L. Chen, X. Yu, Y. Wang and G. Zheng, *Advanced Energy Materials*, 2017, **7**, 1601390.
8 Z. Peng, D. Jia, A. M. Al-Enizi, A. A. Elzatahry and G. Zheng, *Advanced Energy Materials*, 2015, **5**, 1402031.
9 J. White, I. Terekhina, E. Campos Dos Santos, D. Martín-Yerga, L. G. M. Pettersson, M. Johnsson and A. Cornell, *ACS Appl. Energy Mater.*, 2024, **7**, 1802–1813.
10 A. Cassani, N. Tuleushova, Q. Wang, H. Guesmi, V. Bonniol, J. Cambedouzou, S. Tingry, M. Bechelany, D. Cornu and Y. Holade, *ACS Appl. Energy Mater.*, 2021, **4**, 9944–9960.
11 C. R. Zanata, C. A. Martins, É. Teixeira-Neto, M. J. Giz and G. A. Camara, *Journal of Catalysis*, 2019, **377**, 358–366.
12 M. Weber, P. Collot, H. El Gaddari, S. Tingry, M. Bechelany and Y. Holade, *ChemElectroChem*, 2018, **5**, 743–747.
13 D. Xu, Y. Liu, S. Zhao, Y. Lu, M. Han and J. Bao, *Chem. Commun.*, 2017, **53**, 1642–1645.
14 R. G. Da Silva, S. Aquino Neto, K. B. Kokoh and A. R. De Andrade, *Journal of Power Sources*, 2017, **351**, 174–182.
15 Y. Kang, W. Wang, Y. Pu, J. Li, D. Chai and Z. Lei, *Chemical Engineering Journal*, 2017, **308**, 419–427.
16 J. González-Cobos, S. Baranton and C. Coutanceau, *ChemElectroChem*, 2016, **3**, 1694–1704.
17 S. Li, J. Lai, R. Luque and G. Xu, *Energy Environ. Sci.*, 2016, **9**, 3097–3102.
18 A. Zalineeva, A. Serov, M. Padilla, U. Martinez, K. Artyushkova, S. Baranton, C. Coutanceau and P. B. Atanassov, *J. Am. Chem. Soc.*, 2014, **136**, 3937–3945.
19 J. Tang, X. Zhao, Y. Zuo, P. Ju and Y. Tang, *Electrochimica Acta*, 2015, **174**, 1041–1049.
20 Y. Holade, C. Morais, K. Servat, T. W. Napporn and K. B. Kokoh, *ACS Catal.*, 2013, **3**, 2403–2411.
21 A. Serov, U. Martinez and P. Atanassov, *Electrochemistry Communications*, 2013, **34**, 185–188.
22 M. Simões, S. Baranton and C. Coutanceau, *Applied Catalysis B: Environmental*, 2010, **93**, 354–362.
23 D. Wang, Y. Zhang, K. Zhang, X. Wang, C. Wang, Z. Li, F. Gao and Y. Du, *Journal of Colloid and Interface Science*, 2023, **650**, 350–357.
24 S. Li, J. Shu, S. Ma, H. Yang, J. Jin, X. Zhang and R. Jin, *Applied Catalysis B: Environmental*, 2021, **280**, 119464.
25 Z. Li, Y. Chen, G. Fu, Y. Chen, D. Sun, J.-M. Lee and Y. Tang, *Nanoscale*, 2019, **11**, 2974–2980.
26 H. Lv, Y. Wang, A. Lopes, D. Xu and B. Liu, *Applied Catalysis B: Environmental*, 2019, **249**, 116–125.

27 Y. Chen, Z. Fan, Z. Luo, X. Liu, Z. Lai, B. Li, Y. Zong, L. Gu and H. Zhang, *Advanced Materials*, 2017, **29**, 1701331.
28 R. Jana, U. Subbarao and S. C. Peter, *Journal of Power Sources*, 2016, **301**, 160–169.
29 K. Zhang, D. Bin, B. Yang, C. Wang, F. Ren and Y. Du, *Nanoscale*, 2015, **7**, 12445–12451.
30 C. Hu, X. Zhai, Y. Zhao, K. Bian, J. Zhang, L. Qu, H. Zhang and H. Luo, *Nanoscale*, 2014, **6**, 2768.
31 C. Zhu, S. Guo and S. Dong, *Advanced Materials*, 2012, **24**, 2326–2331.
32 H. Chen, X. Wu, D. Liu, C. Ye, L. Huang, X. Long, L. Wang, J. Zhang, J.-L. Luo and X.-Z. Fu, *Chemical Engineering Journal*, 2023, **474**, 145639.
33 H. Fu, N. Zhang, F. Lai, L. Zhang, S. Chen, H. Li, K. Jiang, T. Zhu, F. Xu and T. Liu, *ACS Catal.*, 2022, **12**, 11402–11411.
34 J. Li, X. Wang, C. Xing, L. Li, S. Mu, X. Han, R. He, Z. Liang, P. Martinez, Y. Yi, Q. Wu, H. Pan, J. Arbiol, C. Cui, Y. Zhang and A. Cabot, *Chemical Engineering Journal*, 2022, **440**, 135817.
35 Y. Xu, M. Liu, S. Wang, K. Ren, M. Wang, Z. Wang, X. Li, L. Wang and H. Wang, *Applied Catalysis B: Environmental*, 2021, **298**, 120493.
36 Y. Zhu, X. Zhu, L. Bu, Q. Shao, Y. Li, Z. Hu, C. Chen, C. Pao, S. Yang and X. Huang, *Adv Funct Materials*, 2020, **30**, 2004310.
37 Y. Li, X. Wei, L. Chen, J. Shi and M. He, *Nat Commun*, 2019, **10**, 5335.
38 G.-F. Chen, Y. Luo, L.-X. Ding and H. Wang, *ACS Catal.*, 2018, **8**, 526–530.